Hindawi
International Journal of Antennas and Propagation
Volume 2022, Article ID 9669114, 14 pages
https://doi.org/10.1155/2022/9669114

Research Article

Characteristic Mode-Based Neutralization Line Design for MIMO Antenna

Yitian Sun,[1] Minmin Tian,[1] and G. S. Cheng[1,2,3]

[1]*Information Materials and Intelligent Sensing Laboratory of Anhui Province, Anhui University, Hefei 230601, China*
[2]*Anhui Province Key Laboratory of Target Recognition and Feature Extraction, Lu'an 237010, China*
[3]*Chizhou XRF Electronic Technology Co. Ltd., Chizhou 247100, China*

Correspondence should be addressed to G. S. Cheng; gscheng89@ahu.edu.cn

Received 28 February 2022; Revised 2 May 2022; Accepted 23 June 2022; Published 30 July 2022

Academic Editor: Hervé Aubert

Based on the theory of characteristic modes (TCMs), this paper proposes a systematic design procedure to guide the design of a neutralization line (NL) for a dual-band multiple-input-multiple-output (MIMO) antenna to achieve high isolation. According to the direction of the current flow of significant characteristic modes, coupling and uncoupling modes are identified and a metal NL is appropriately designed to cancel the coupling modes. More specifically, it introduces new currents opposite in direction to the original coupling characteristic currents, thus reducing mutual coupling. Compared with the traditional NL design method, the proposed approach simplifies the optimization process and saves lots of optimal design time. As an illustration of the proposed design method, we design another dual-band antenna operating in the WLAN bands with a compact size of 50 mm × 48 mm × 0.8 mm and minimum edge-to-edge space between the radiating elements with $0.033\lambda_0$ of the lower band. The impedance bandwidths for $S_{11} \leq -10$ dB are 0.42 GHz (2.27–2.69 GHz) and 0.24 GHz (5.6–5.84 GHz). A fabricated prototype shows good agreement between the measured and simulated results. The introduced NL improves the isolation degree by about 18 dB for the 5.8 GHz band, and the total efficiency of the antenna was also improved. In addition, the proposed antenna also has a low envelop correlation coefficient (ECC < 0.3), high diversity gains, and low total active reflection coefficient (TARC) in the frequency band of interest. Measurement results show that the proposed MIMO antenna system is suitable for WLAN applications.

1. Introduction

With the rapid development of wireless communication, how to use the limited spectrum resources to improve the communication quality and signal transmission rate in a harsh environment has always been a hot spot, and multiple-input multiple-output (MIMO) technology is one of the most promising solutions. MIMO system adopts multiple antennas or antenna arrays at both ends of the transceiver, which can provide an additional degree of freedom to increase channel capacity, ensure communication quality, and improve transmission rate by utilizing the multipath characteristics of space channel without increasing transmission power and communication bandwidth [1]. The mutual coupling of antennas on transmitter and receiver should be low for good quality of communication and channel capacity [2].

However, the rapid development of mobile communication equipment makes the space for the integration of antennae becomes smaller and smaller. A load of multiple antennas in a limited space will inevitably produce large mutual coupling, which leads to poor impedance matching and bad diversity performance of the MIMO system. In recent years, researchers have proposed several methods to improve the isolation between antenna elements, such as decoupling networks [3–5], metasurfaces and metamaterials [6–9], electromagnetic-bandgap (EBG) structures [10–14], defective ground structures (DGS) [15–18], split-ring resonators (SRRs) [19], and neutralization line (NL) technique [20–23]. NL technique has been studied extensively because it does not require additional space or changing the ground plane. The working principle of NL is to connect the antenna element with a metal strip and cancel each other out by

introducing a new current in the opposite direction of the original coupling current. However, it is difficult to determine the loading position and the specific parameters of NL, which requires a lot of optimization time.

The theory of characteristic modes (TCM) was studied by Harrington and Mautz [24] and is widely adopted in antenna design [25–35]. One of the most attractive properties of TCM is that both the characteristic current and the characteristic field at infinity satisfy the property of orthogonality. By taking advantage of this property, TCM is widely adopted in the MIMO system because good envelope correlation coefficient (ECC) performance can be realized.

Characteristic mode analysis of two adjacent planar inverted-F antenna (PIFA) elements was reported to show how a shorted line could help reduce the mutual coupling [32]. However, the design of the NL in [32] was still based on the traditional electromagnetic analysis and optimization algorithm. The TCM was only used to analyze and verify why the loaded NL could achieve the effect of decoupling from the perspective of mode theory. In this study, based on the initial preliminary work in [23], a TCM-based design procedure to systematically guide the design of NL is proposed. The characteristic mode analysis is performed for the initial MIMO antenna without NL. According to the direction of the significant characteristic currents, coupling and uncoupling modes are identified. A metal NL is appropriately designed according to the characteristic current distribution of the coupling modes to cancel the mutual coupling. More specifically, the shape of NL is determined qualitatively based on the characteristic currents of the coupling mode. Then, HFSS was used to optimize the critical parameters of NL and determine it quantitatively. Compared with the traditional optimization design method, the proposed TCM-based design procedure can save lots of optimal design time. Experimental results show that 21 dB of isolation between the ports is achieved, and good agreement is observed between the measured and simulated results.

2. Characteristic Mode Analysis and Design Procedure

2.1. Introduction of TCM. The TCM provides a clear physical concept, which can essentially explain the radiation mechanism of an antenna and facilitate the guidance of antenna design, such as the essential physical characteristics of antenna structure and appropriate feed structure as well as the feed location to excite a characteristic mode (CM). More specific derivations of TCM and its application in antenna design are detailed in [33].

The CMs of arbitrarily shaped perfectly electrically conducting (PEC) bodies can be obtained from $\mathbf{X}(\mathbf{J_n}) = \lambda_n \mathbf{R}(\mathbf{J_n})$, where λ_n is eigenvalues, $\mathbf{J_n}$ is eigenvectors or the characteristic currents, and $\boldsymbol{R}$ and $\boldsymbol{X}$ are real and imaginary Hermitian parts of the generalized impedance matrix $\boldsymbol{Z} = \boldsymbol{R} + j\ \boldsymbol{X}$ resulting from electric field integral equation (EFIE) [33]. The eigenvalue λ_n is a handy parameter because it can reveal the resonance and radiation information of its corresponding CM. In fact, there are several other preferred variables that can provide resonance and radiation information. The modal significance (MS), defined as $MS_n = |1/(1+ j\lambda_n)|$, is the inherent and excitation source-independent property of each mode. It converts the variation range of eigenvalues $[-\infty, +\infty]$ to [0, 1]. The characteristic mode is resonant when λ_n is zero, while $MS_n = 1$. The CMs form a complete set of orthogonal modes so that the induced current (J) of a conducting object excited by an excitation source can be expanded as $J = \Sigma\alpha_n J_n$, where α_n is the modal weighting coefficients determined by the MS_n, external excitation source, and characteristic current of the nth mode [33]. In the following section, the TCM analysis of the proposed antennas is carried out using the commercial simulation software FEKO.

2.2. TCM-Based NL Design. Figure 1 shows the initial geometry of a MIMO antenna designed in this paper (named antenna#1), which consists of two symmetric antenna elements. The antenna unit is designed based on the traditional inverted L-shaped monopole antenna. By loading the horizontal radiation branch and bending it, the dual-band and miniaturization characteristics of the antenna are realized, respectively. The antenna is printed on an FR-4 substrate with a relative permittivity of 4.4, a loss tangent of 0.02, and a thickness of 1.6 mm. The antenna size is 54 mm × 32 mm × 1.6 mm.

The S-parameters of the MIMO antenna#1 are illustrated in Figure 2. It can be seen that the mutual coupling without the NL is lower than −15 dB within 2.37–2.69 GHz while higher than −15 dB within 5.0–5.84 GHz. Therefore, an additional decoupling structure is needed to improve the isolation at the high-frequency band.

The initial antenna structure is analyzed by TCM. Figure 3 shows the MS of the significant modes of the antenna. MS is a good indicator to measure the coupling degree between each mode and the external excitation field and determine its radiation performance. In general, the mode with an MS value greater than 0.707 is considered the significant mode that plays an essential role in antenna radiation [33]. As can be seen from Figure 3, mode 1, mode 1' and mode 2' are significant modes at the frequency band of interest.

Figure 4 gives the characteristic current distribution of significant modes. In the low-frequency band, mode 1 has current flowing from left to right, so mode 1 is defined as a coupling mode for this band. However, the coupling of the antenna at the low-frequency band is not strong, and there is no need to deal with it. It can be seen from Figure 4(c) that mode 1' has a large amount of current flowing from the antenna unit on the left to the right, so this mode is defined as a coupling mode at the high-frequency band. Although mode 2' is also a significant mode, it can be seen from the current distribution and flow direction (Figure 4(e)) that there is no current coupling between the two antenna elements, so this mode is defined as the uncoupling mode.

According to the characteristic currents of the coupling mode shown in Figure 4(c), the shape and loading position of NL is determined qualitatively, and different heights of arc NLs are loaded based on the coupling characteristic mode

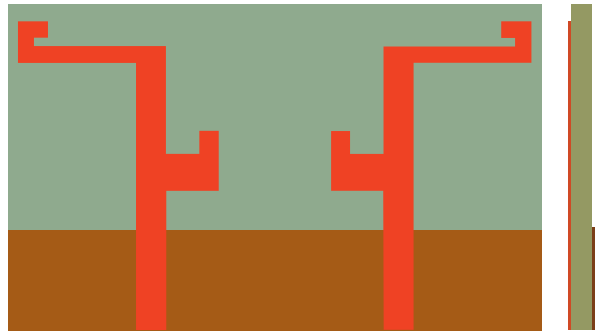

Figure 1: Structure of antenna#1 without NL: (a) perspective view and (b) end view.

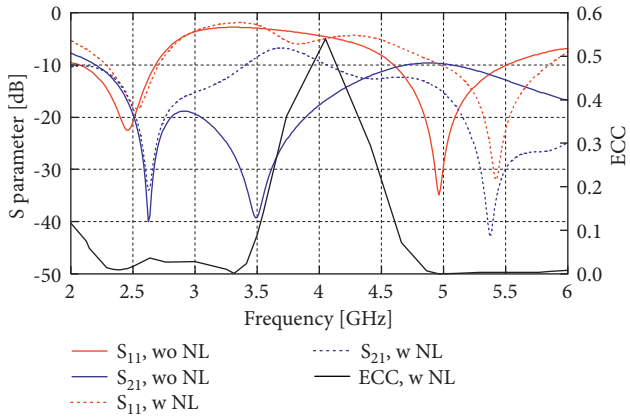

Figure 2: Simulation of ECC (with NL) and S-parameters of antenna#1 with and without NL.

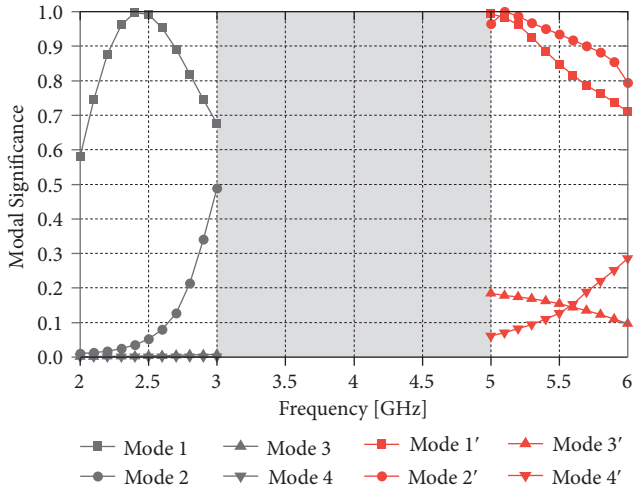

Figure 3: MS for the dominant CMs of the MIMO antenna#1 without the NL.

currents, just as is shown in Figure 5. The next step is to determine the specific parameters of NL quantitatively, and then the key parameters (H, W) of NL shown in Figure 5(a) are optimized using commercial software HFSS based on the antenna's S parameter. The optimization process is given.

The variable H represents the height of NL. With the decrease of H, the resonance frequency, impedance matching, and isolation of the antenna at the low-frequency band do not change much, as shown in Figure 6. This is consistent with our original design. Just as can be observed from comparing characteristic currents before and after loading NL in Figures 4(a) and 4(b), the characteristic current at the low-frequency band does not change much after adding the NL. Therefore, the loaded NL will not affect the antenna of the low-frequency part too much. While at the high-frequency band, with the decrease of parameter H, the resonant frequency shifts to the right, but the bandwidth of S_{11} does not change much. The S_{21} decreases first and then increases, which means the isolation of the antenna gets better at first and then gets worse. The H value is determined from 10 mm to 11 mm based on the above analysis, and by further optimization, the optimal value of H is chosen as 10.1 mm.

Similarly, the width (W) of the NL has almost no effect on the S-parameters at the low frequency, as shown in Figure 7. While at the high-frequency band, with the increase of W, S_{11} slightly shifts to high frequency, and S_{21} becomes better first and then becomes worse. Reasonable compromise based on the S_{11} and S_{21}, the optimal value of W is chosen as 0.5 mm based on the parameter scan result.

So parameters H and W mainly influence the antenna's performance on the high-frequency band and have little influence on the low-frequency band, which is consistent with our analysis based on characteristic currents. The optimal values of H and W are chosen as 0.1 mm and 0.5 mm, respectively.

The antenna#1 loaded with NL is shown in Figure 5. The addition of NL changes the surface current distribution of the radiation element and thus affecting the matching of the antenna, just as shown in Figure 2. To compensate for this effect, the high-frequency radiation unit is designed to resonate at 5 GHz so that after the addition of NL, the resonance frequency of the whole antenna will be around the desired frequency of 5.5 GHz. It should be mentioned that although the distribution of characteristic current changes with the change of frequency, the distribution of characteristic current will remain relatively stable when the change of frequency is relatively small. In other words, we can still

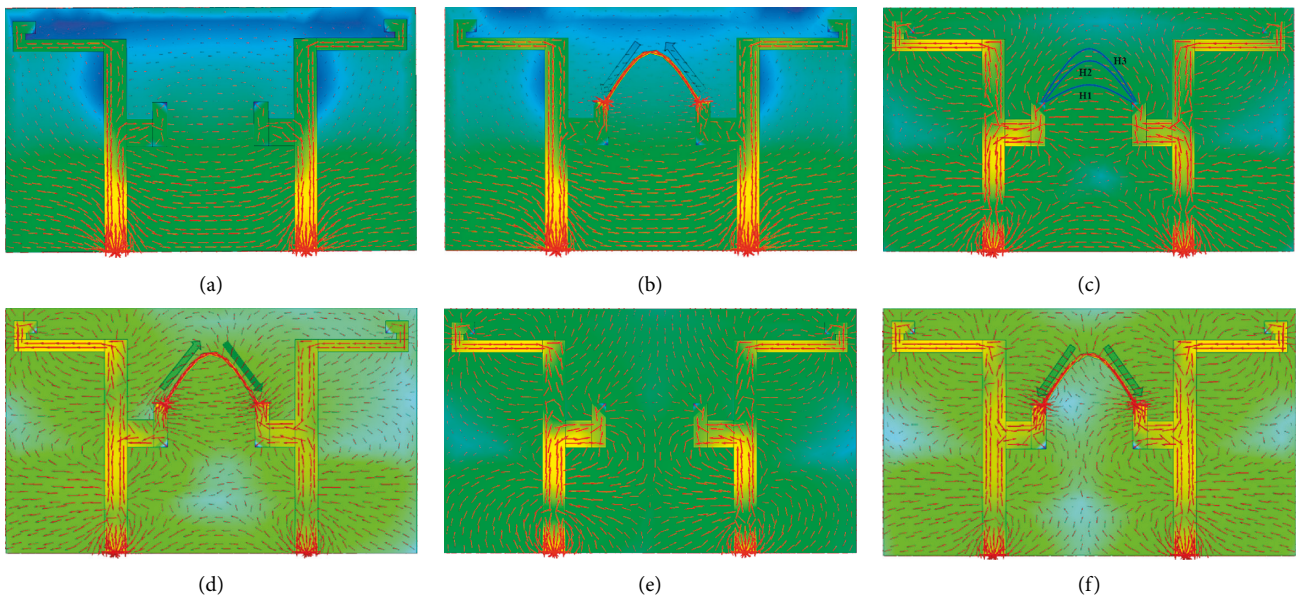

Figure 4: Characteristic current distribution of the significant modes of antenna#1: (a) mode 1 at 2.45 GHz, (b) mode 1 at 2.45 GHz, (c) mode 1' at 5.5 GHz, (d) mode 1' at 5.5 GHz, (e) mode 2' at 5.5 GHz, and (f) mode 2′ at 5.5 GHz.

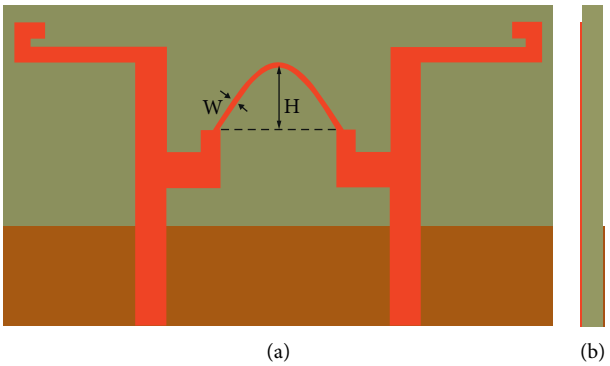

Figure 5: Structure of antenna#1 with NL: (a) perspective view and (b) end view.

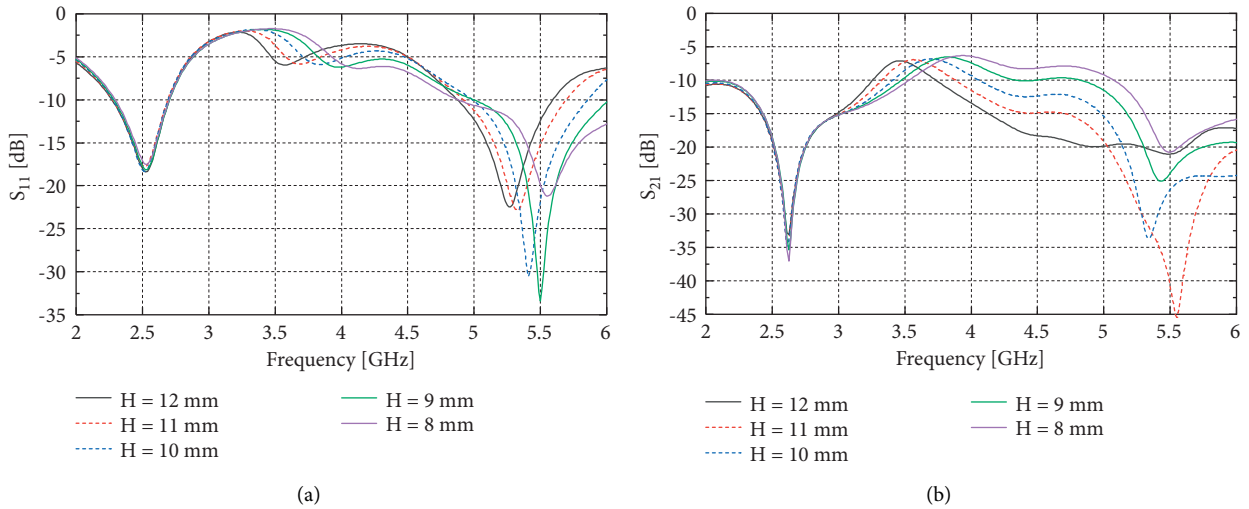

Figure 6: S-parameters of antenna#1 with different heights of the NL: (a) S_{11} and (b) S_{21}.

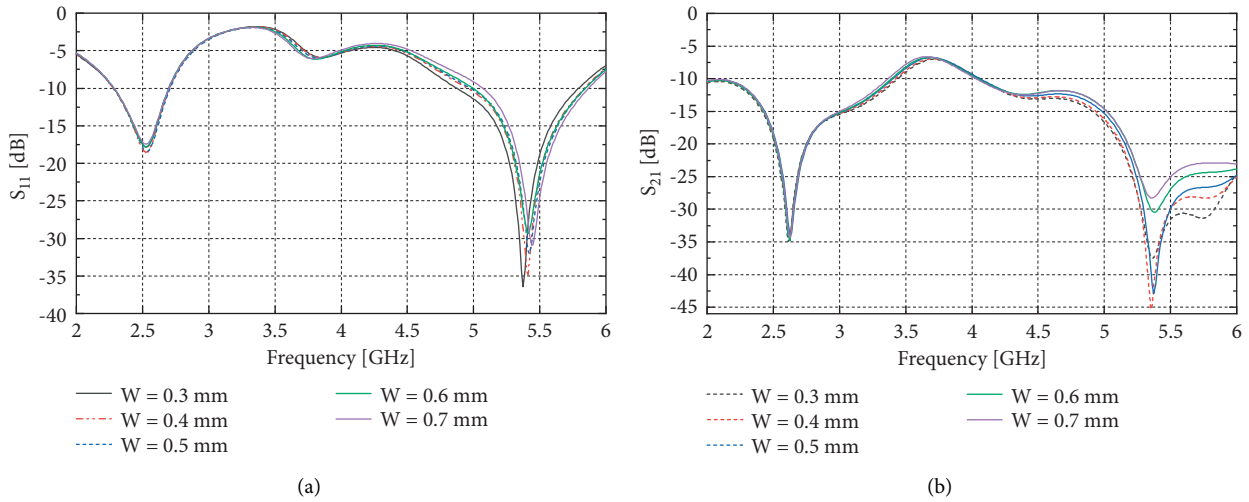

Figure 7: S-parameters of antenna#1 with different widths of the NL: (a) S_{11} and (b) S_{21}.

qualitatively guide the design of the NL (parameters such as position and shape) according to the characteristic current distribution of the coupling mode at the resonant frequency point of the original structure (without NL).

Figures 4(b), 4(d), and 4(f) show the characteristic current distribution of the antenna after adding NL. It can be seen that the loaded NL introduces a new current, whose current direction is opposite to that of the coupling mode (the directions of the mode current on the NL are indicated by gray arrows). It can also be seen from the distribution of characteristic current that the original coupling mode becomes uncoupling mode after the NL is added. This indicates that the loaded NL can improve the isolation effectively, just as shown in Figure 2. Results show that the isolation in the high-frequency band is improved by about 25 dB, and the low-frequency part is also improved a little. In addition, ECCs of the antenna were less than 0.3 in the working frequency bands, which means the MIMO antenna has good diversity gain performances [36, 37].

3. Another Similar Antenna Design and Porotype Verification

3.1. Design of Another Dual-Band Antenna. Using the same design method, a more complex MIMO antenna is designed and processed, which covers the 2.4 GHz and 5.8 GHz bands of WLAN.

Similarly, the antenna unit is also composed of a bent monopole structure. The geometry of the antenna is depicted in Figure 8 (named antenna#2). The left bend branch works at low frequency, while the right bend branch works at high frequency. The low-frequency part uses the antenna layout to obtain a good isolation degree, while the high-frequency part introduces the NL technology to improve the isolation degree. The antenna is also printed on an FR-4 dielectric substrate with a relative dielectric constant of 4.4 and a loss tangent angle of 0.02. The overall size is 50 mm × 48 mm, and the thickness is 0.8 mm.

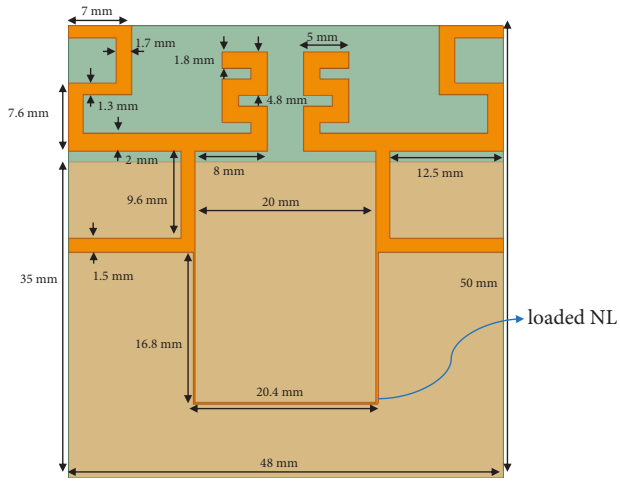

Figure 8: Overall structure of the MIMO antenna#2.

The S-parameters of antenna#2 with and without loading NL are shown in Figure 9. It can be seen that after the NL is loaded, the isolation of the antenna changes little at 2.4 GHz but increases by about 18 dB at 5.8 GHz.

To confirm the design idea of using TCM to improve mutual coupling and the working mechanism of NL proposed above, the characteristic currents of significant modes for the antenna at 2.45 GHz and 5.8 GHz are given in Figure 10. The significant mode at low frequency is mode 1. As can be seen from Figure 10(a), the characteristic current flow at 2.45 GHz is mainly from top to bottom, so there is very weak current coupling between antenna units, which indicates that the antenna has good isolation at low frequency.

As is shown in Figure 10(d), after the NL is added, characteristic current on NL cancels out, indicating that the isolation of the antenna at the low-frequency band will not change much. Figures 10(b) and 10(c) show the significant modes' current distribution of the antenna at the high-frequency band; it is observed that the coupling between the

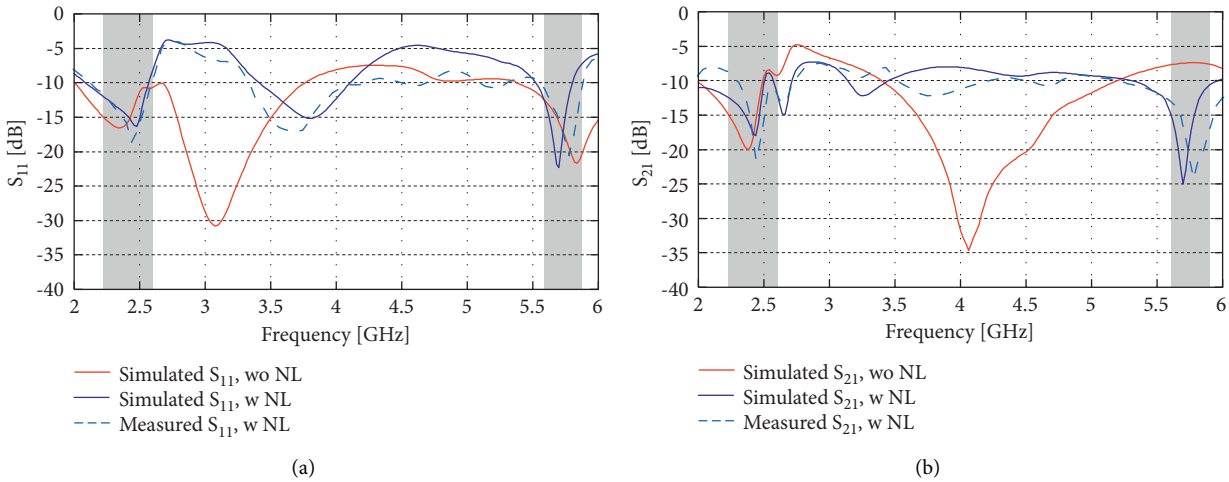

FIGURE 9: S-parameters of antenna#2 with and without NL: (a) S_{11} and (b) S_{21}.

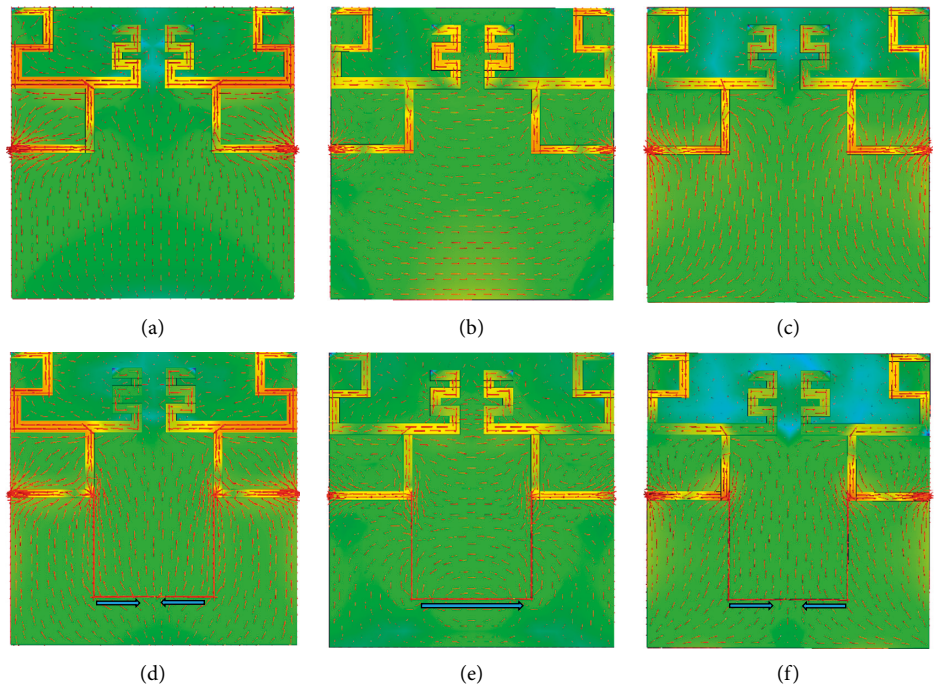

FIGURE 10: Characteristic current distribution of the significant modes of antenna#2: (a) mode 1 at 2.45 GHz, (b) mode 2 at 5.8 GHz, (c) mode 3 at 5.8 GHz, (d) mode 1 at 2.45 GHz, (e) mode 2 at 5.8 GHz, and (f) mode 3 at 5.8 GHz.

antenna unit is mainly caused by mode 2. The current flow of mode 3 is primarily from top to bottom, just like mode 1, and has little effect on coupling. So mode 2 is defined as coupling mode, and mode 3 is defined as uncoupling mode. The loaded NL should generate a current flow in the opposite direction to mode 2 to achieve a decoupling effect.

According to the direction of characteristic currents of mode 2 shown in Figure 10(b), the shape and loading position of NL are determined qualitatively, just as shown in Figure 11. The next step is to determine the specific parameters of NL quantitatively, and then the key parameters (*offset*, *L*) of NL shown in Figure 11 are optimized using commercial software HFSS.

The influences of the loading position of NL (*offset*) and the length of NL (*L*) on the S-parameter are analyzed. The variable *offset* represents the loading position of NL relative to the port. As can be seen from Figure 12, for the low-frequency band, with the increase of *offset*, the loading position of the NL is gradually away from the port; the bandwidth of S_{11} becomes wider; and the isolation becomes better. While for the high-frequency band, the notch curves of S_{11} and S_{21} move to high-frequency gradually with the increase of *offset*. So there is an optimal solution for variable *offset*, making the antenna cover the 5.8 GHz band and obtain an isolation degree greater than 15 dB in this band. We choose the optimal value of *offset* = 14 mm.

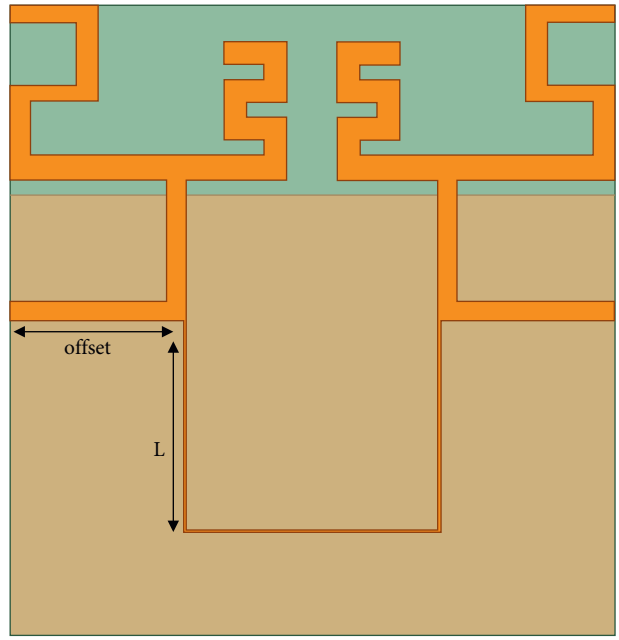

Figure 11: Structure of antenna#2 with NL.

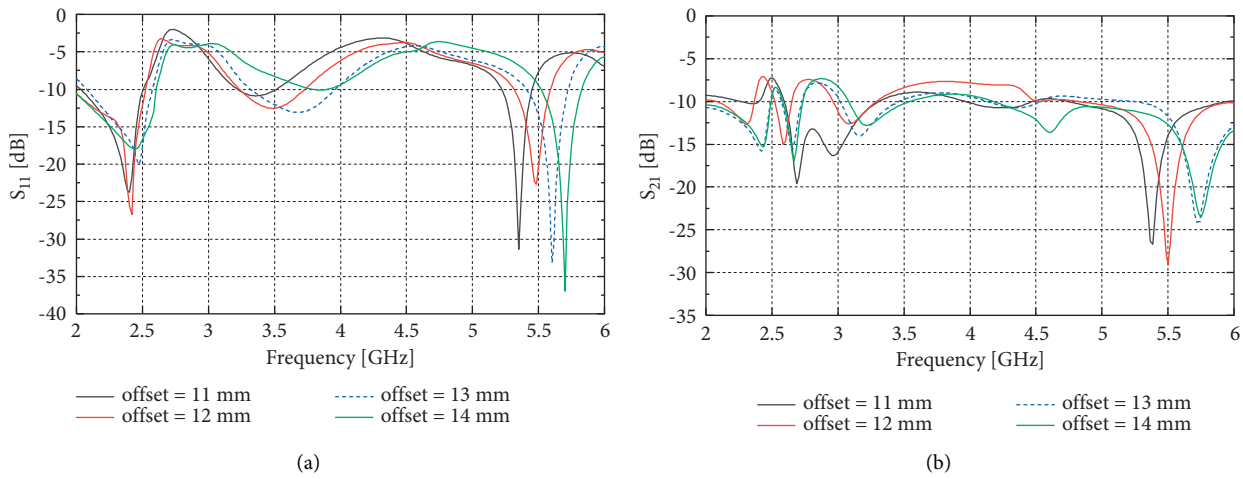

Figure 12: S-parameter of antenna#2 with different *offsets* of the NL: (a) S_{11} and (b) S_{21}.

The variable L represents the length of NL. As can be seen from Figure 13, for the low-frequency band, with L increase from 15 mm to 18 mm, impedance matching is improved, but it has almost no effect on S_{21}. That is because the NL is loaded far away from the port, and the current on NL is weak. No matter how the length of NL changes, the current on the NL will always be weak, so L does not have much effect on S_{21} for the low-frequency band. For the high-frequency band, L has a significant influence on both S_{11} and S_{21}, just as shown in Figure 13. As the variable L increases, the resonant point at the high-frequency band shifts to low frequency. Similarly, as the value of L increases, the notch curve of S_{21} moves towards low frequency. Therefore, variable L has an optimal value to cover the 2.4 GHz and 5.8 GHz bands effectively. By further optimization, the optimal value of L is chosen as 16.8 mm.

The characteristic current distribution after adding NL is shown in Figures 10(d), 10(e), and 10(f). As mentioned before, it has little influence on the antenna at the low-frequency band. The coupling of the antenna is mainly generated by mode 2. After adding NL, it can be seen from Figure 10(e) that part of the current that used to flow from the left to the right of the antenna becomes a loop current. Moreover, the current generated on NL flows in opposite direction to the current causing coupling, indicating that the added NL can improve the isolation of the antenna effectively. For modes 1 and 3, the currents generated on NL cancel each other out, with little effect on antenna isolation. It is consistent with Figure 9; the isolation in the 5.8-GHz band improved a lot while in the 2.4 GHz band did not change much. Figure 14 displays the radiation patterns of MIMO antenna with and without NL; the loaded NL will

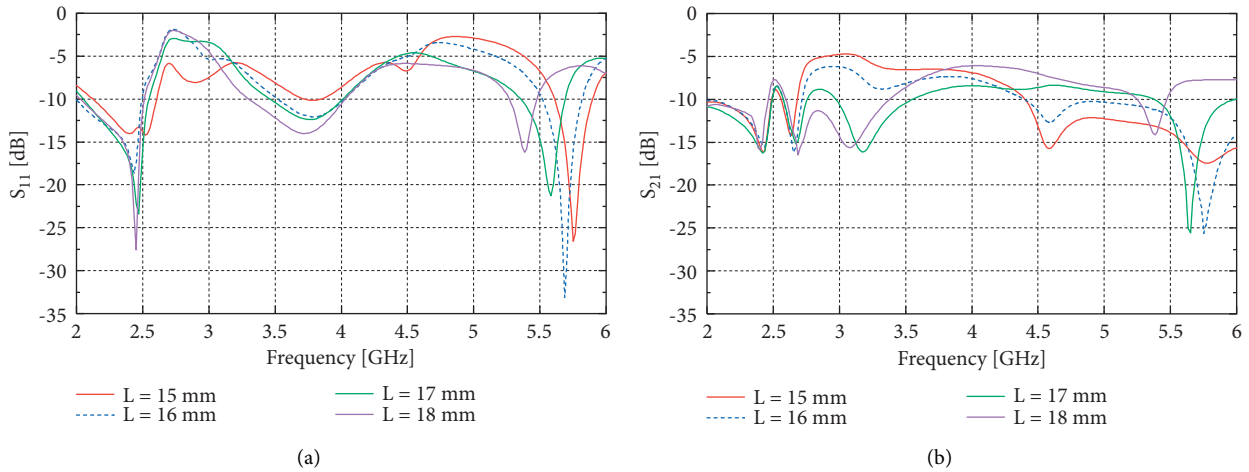

Figure 13: S-parameter of antenna#2 with different lengths of the NL: (a) S_{11} and (b) S_{21}.

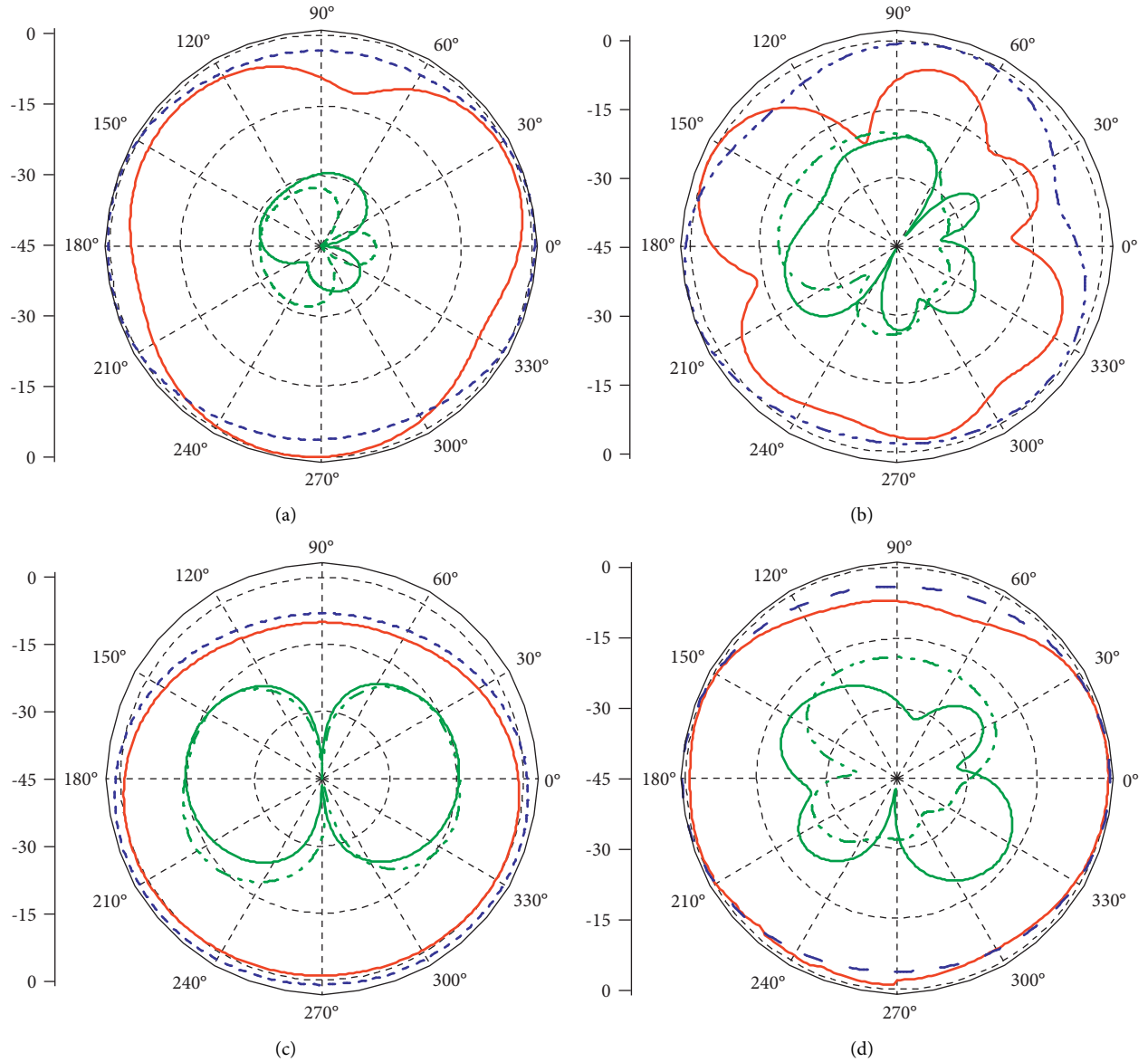

Figure 14: Simulated normalized radiation patterns of antenna #2 with and without NL. —G_θ with NL, —G_Φ with NL, —G_θ without NL, and - - -G_Φ without NL. (a) *xz*-plane at 2.4 GHz, (b) *xz*-plane at 5.8 G, (c) *yz*-plane at 2.4 GHz, and (d) *yz*-plane at 5.8 GHz.

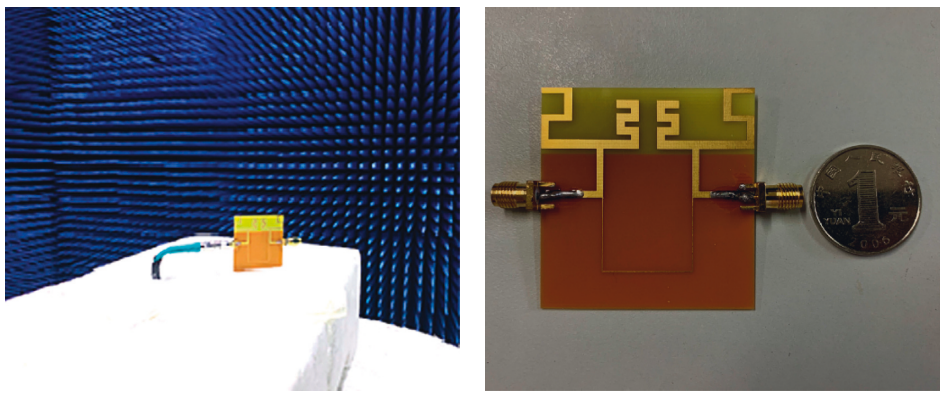

(a) (b)

Figure 15: Fabricated prototype of the dual-band antenna#2: (a) testing environment and (b) front view.

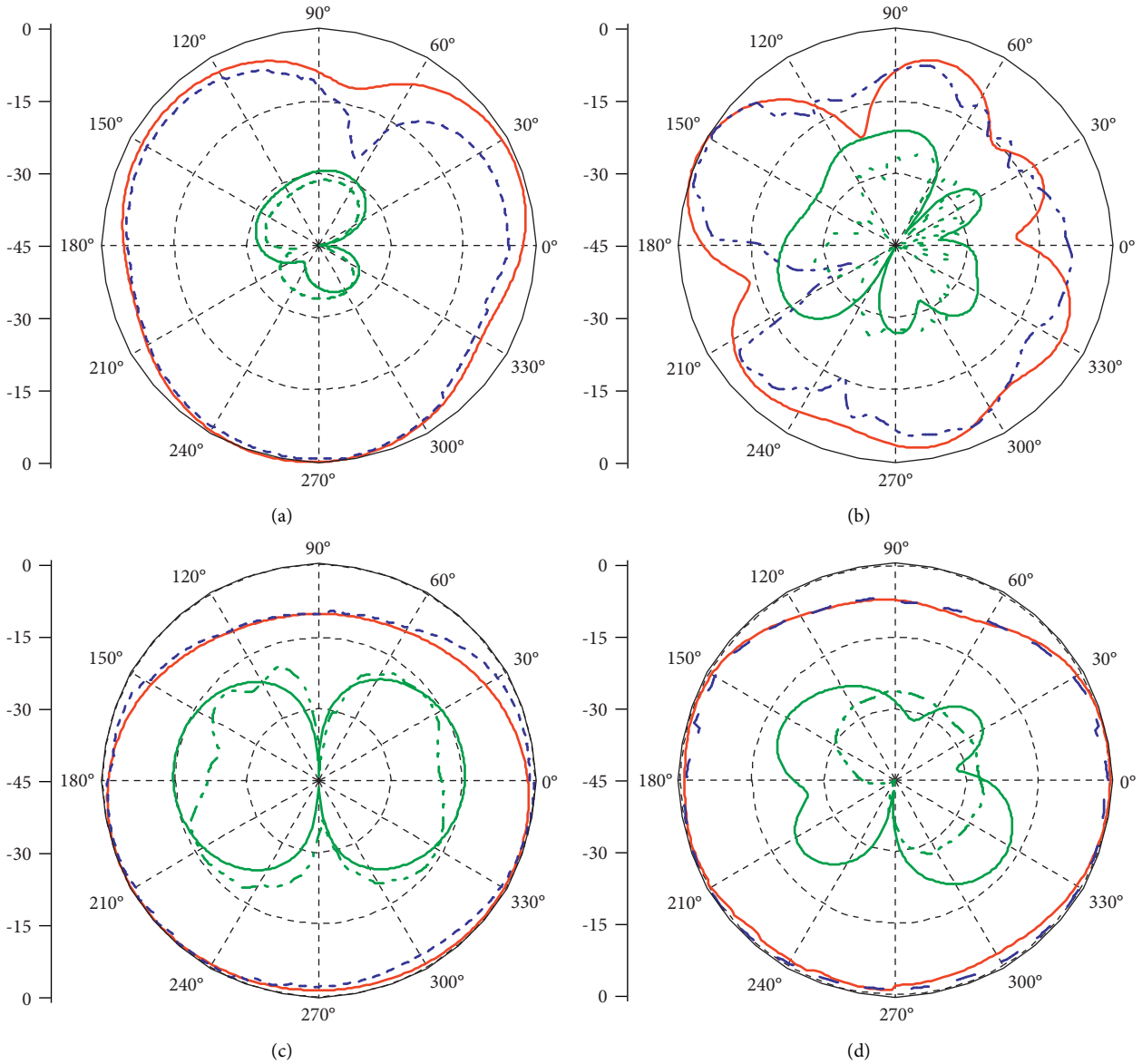

Figure 16: Simulated and measured normalized radiation patterns of antenna#2 at 2.4 GHz and 5.8 GHz. — HFSS G_θ, — HFSS G_Φ, - - - Meas G_θ, and - - - - Meas G_Φ. (a) *xz*-plane at 2.4 GHz, (b) *xz*-plane at 5.8 GHz, (c) *yz*-plane at 2.4 GHz, and (d) *yz*-plane at 5.8 GHz.

Table 1: Comparison of the radiation efficiency and total efficiency of antenna#2 w/wo NL.

	At low frequency		At high frequency	
	Radiation efficiency (%)	Total efficiency (%)	Radiation efficiency (%)	Total efficiency (%)
wo NL	94.9	86.0	87.3	69.9
w NL	93.5	87.0	86.7	76.0

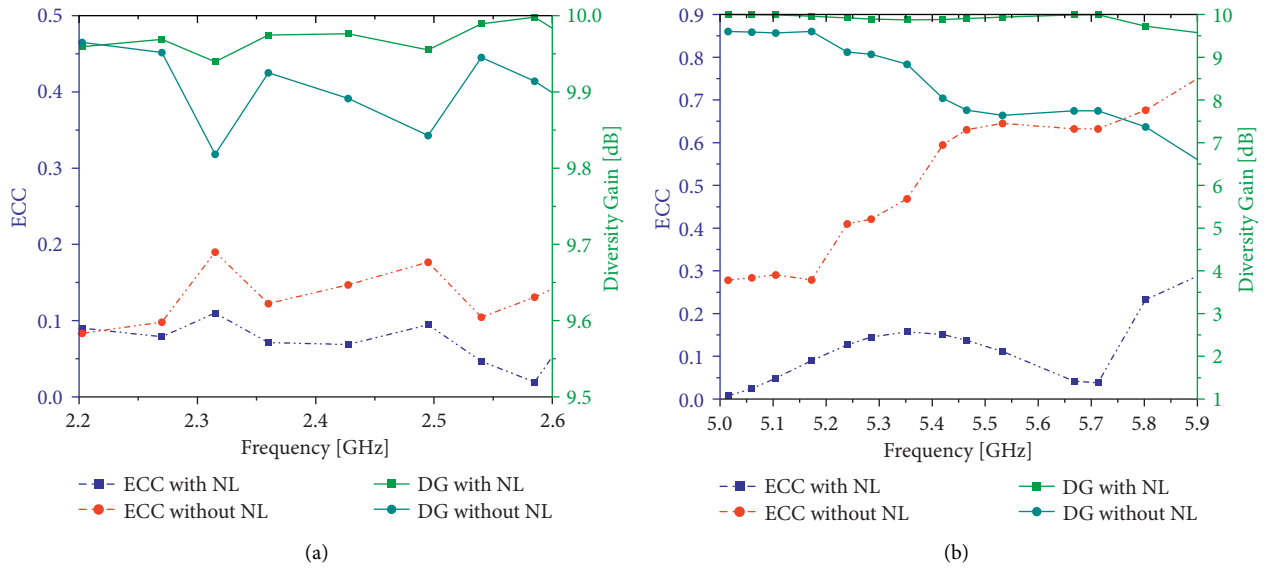

Figure 17: The ECC and DG of the proposed antenna#2 with and without NL: (a) 2.4 GHz and (b) 5.8 GHz.

have some effect on the far-field patterns and slightly distort the radiation pattern for the *xz*-plane in the 5.8 GHz band.

3.2. Experimental Results and Discussion. The proposed dual-band MIMO antenna#2 has been fabricated as shown in Figure 15. The S-parameters have been measured with a vector network analyzer. As can be seen from Figure 9, the measured result is consistent with the simulated one. There is a slight shift at the higher resonant frequency, possibly due to the fabrication and experimental tolerances.

Figure 16 displays the simulated and measured normalized radiation patterns of antenna#2 (one monopole is excited, while the other is terminated with a 50 Ω load) at 2.4 GHz and 5.8 GHz, and a good agreement is observed. The slight differences are caused by the influences of feed cables and the misalignment of the antenna resonant frequency. It can be observed that both *xz* and *yz* planes have similar omnidirectional radiation patterns, which means the antenna can receive or transmit signals from all directions.

The radiation efficiency and total efficiency of antennas#2 with and without NL are compared in Table 1. As shown in Table 1, the radiation efficiencies of the antennas at both bands are almost equal to 90%. Thus, the loaded NL reduces the mutual coupling to decrease the correlation of the two elements to maximize the MIMO performance without introducing additional loss to the radiation efficiency. Moreover, the proposed NL can efficiently enhance the isolation at a high frequency between MIMO elements so that the total efficiency at the high frequency of the proposed MIMO antennas can be improved. The total efficiency improvement with the NL is observed clearly at high frequency, while there is no significant change at low frequencies. The relationship between total efficiency and radiant efficiency is as follows:

$$\eta_{\text{total}} = \eta_{\text{rad}}\left(1 - \left|S_{11}\right|^2 - \left|S_{21}\right|^2\right). \tag{1}$$

To further validate the capability and performance of MIMO antenna#2, the envelope correlation coefficient (ECC), diversity gain (DG), total active reflection coefficient (TARC), and mean channel capacity have been evaluated.

The pattern diversity performance of MIMO antenna#2 can be evaluated by the ECC, which is an important parameter to measure the fading ability of the antenna signal and signal transmission rate [36, 37]. The ECC calculation method adopted in this paper is based on radiation patterns given by (2), where $\mathbf{F}_i(\theta, \varphi)$ or $\mathbf{F}_j(\theta, \varphi)$ means the far-field radiation patterns of the antenna i or j fed separately while other ports were connected with matching loads.

$$\rho_c(i, j) = \frac{\left|\iint_{4\pi}\left[\mathbf{F}_i(\theta, \varphi) \cdot \mathbf{F}_j^*(\theta, \varphi) d\Omega\right]\right|^2}{\iint_{4\pi}\left|\mathbf{F}_i(\theta, \varphi)\right|^2 d\Omega \cdot \iint_{4\pi}\left|\mathbf{F}_j(\theta, \varphi)\right|^2 d\Omega.} \tag{2}$$

The DG of the proposed MIMO antenna can be calculated using (3) to evaluate the diversity performance of the

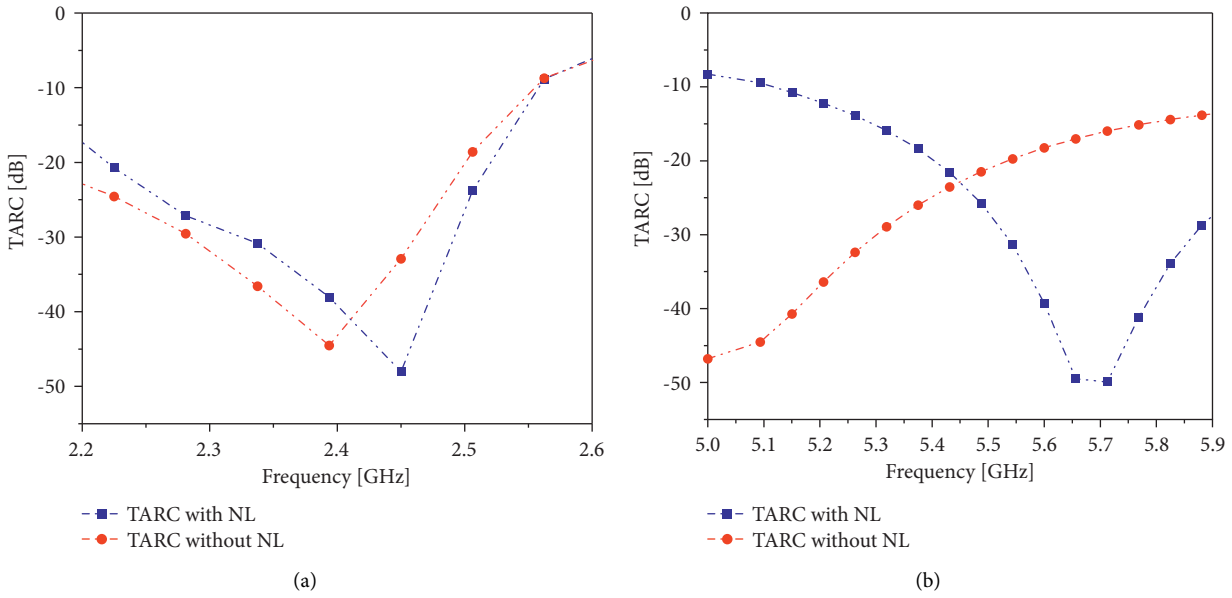

Figure 18: The TARC of antenna#2 with and without NL: (a) 2.4 GHz and (b) 5.8 GHz.

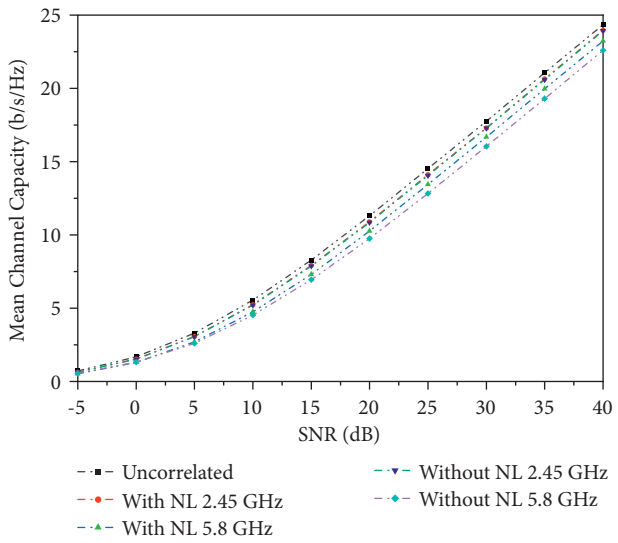

Figure 19: The mean channel capacities of antenna#2 with and without NL.

proposed antenna [38]. Figure 17 shows the measured ECC and DG of antenna#2 with and without loading NL. It can be observed that the loaded NL significantly improves the ECC and DG values of the proposed antenna at the high-frequency band. Furthermore, the ECC was below 0.3 across both bands, which is suitable for MIMO applications, and the DG of the antenna is larger than 9.5 dB in the frequency band of interest.

$$\mathrm{DG} = 10\sqrt{1 - \mathrm{ECC}^2}. \tag{3}$$

TARC is defined as the ratio of the square root of total reflected power divided by the square root of total incident power [38, 39]. The TARC of the 2-port MIMO antenna can be calculated from the S-parameters using the following formula:

$$\mathrm{TARC} = \sqrt{\frac{(S_{11} + S_{12})^2 + (S_{21} + S_{22})^2}{2}}. \tag{4}$$

The measured values of TARC are shown in Figure 18. It is observed from Figure 18 that the loaded NL obviously improves the TARC value of the proposed antenna at dual frequency bands and the value of TARC for the proposed antenna is less than −30 dB for the working frequency bands.

The mean channel capacities of antenna#2 with and without NL as a function of the SNR at 2.45 GHz and 5.8GHz are shown in Figure 19 [37]. It can be seen that the mean

Table 2: Performance comparisons with the previously published literature.

Ref.	Decoupling method	Max decoupling improvement	Number of ports	Bandwidth	Bands	Edge-to-edge distance	Complexity
[3]	Decoupling network	15 dB	2	Narrow	Single	$0.055\lambda_0$	Yes
[5]	Decoupling network	10 dB	2	Wide	Single	$0.084\lambda_0$	Yes
[8]	Metamaterial	32 dB for X-band 27 dB for ku-band 26 dB for K-band	4	Wide	Six	$0.26\lambda_0$	Yes
[9]	Fractal metamaterial EBG	17 dB for S_{12} 37 dB for S_{13} 17 dB for S_{14}	4	Wide	Three	$0.5\lambda_0$	Yes
[12]	EBG	10 dB	2	Narrow	Single	$0.5\lambda_0$	Yes
[13]	Uniplanar compact EBG	14 dB	2	Narrow	Single	$0.5\ \lambda_0$	Yes
[14]	Fractal UC-EBG	16 dB	2	Narrow	Single	$0.22\lambda_0$	Yes
[17]	DGS	40 dB	2	Narrow	Single	$0.031\lambda_0$	No
[18]	DGS	17.4 dB	2	Narrow	Single	$0.23\lambda_0$	No
[19]	SRR	10 dB	2	Narrow	Single	$0.25\lambda_0$	Yes
[21]	NL	23.7 dB	2	Wide	Single	$0.079\lambda_0$	No
[22]	NL	16 dB	2	Narrow	Single	$0.114\lambda_0$	No
This work	TCM + NL	18 dB	2	Narrow	Two	$0.033\lambda_0$	No

channel capacities of the antenna with and without NL are nearly the same at 2.45 GHz and slightly lower than the ideal uncorrelated MIMO configuration. However, for the 5.8GHz band, the mean channel capacity becomes better and closer to the ideal uncorrelated configuration after loading NL.

Finally, to highlight the advantages and innovation of the proposed antenna, comparisons between the proposed antenna and the state-of-the-art MIMO antenna are given in Table 2. The comparison almost represents the current state-of-the-art decoupling technology for MIMO antenna, although it is not comprehensive. The comparison results show that the antenna achieves a good balance in size, isolation, bandwidth, edge-to-edge distance, number of ports, and technical complexity.

4. Conclusions

A TCM-based design procedure is proposed for the design of an NL in MIMO antenna configuration. By analyzing the characteristic current direction of the initial antenna structure, the coupling mode is first identified, and the form and position of the NL were determined qualitatively based on the characteristic currents of the coupling mode. Then, HFSS was used to optimize the critical parameters of NL and determine it quantitatively. Finally, a designed NL is loaded to introduce opposite currents to the coupling mode currents, thus reducing mutual coupling. The measured results of the fabricated prototype show that the isolation of antenna #2 at 5.8 GHz is improved by about 18 dB through adding NL, and the total efficiency has also been improved (69.9% to 76.0%); the impedance bandwidths of the antenna for $S_{11} \leq$ -10 dB are 16.9% (2.27–2.69 GHz) and 4.2% (5.6–5.84 GHz), respectively; the ECC is less than 0.3 in the operating frequency bands. The results are in reasonable agreement between measured and simulated results, demonstrating that the proposed TCM-based design procedure for NL can be used in other MIMO antenna designs.

Data Availability

The data used to support the findings of this study are available from the corresponding author upon request.

Disclosure

Portions of this work were presented at the International Applied Computational Electromagnetics Society (ACES-China) Symposium in 2021, "Characteristic Mode Analysis of Neutralization Line for MIMO Antenna Designs." This submission has been expanded and revised, adding more detailed design steps and experimental data to the conference proceedings.

Conflicts of Interest

The authors declare that there are no conflicts of interest regarding the publication of this paper.

Acknowledgments

This work was supported in part by the National Natural Science Foundation of China under Grant 61901002, in part by the Natural Science Foundation of Anhui Province under Grant 1908085QF258, and in part by the State Key Laboratory of Millimeter Waves Foundation under Grant K202007.

References

[1] M. A. Jensen and J. W. Wallace, "A review of antennas and propagation for MIMO wireless communications," *IEEE*

Transactions on Antennas and Propagation, vol. 52, no. 11, pp. 2810–2824, 2004.

[2] S. Sanayei and A. Nosratinia, "Antenna selection in MIMO systems," *IEEE Communications Magazine*, vol. 42, no. 10, pp. 68–73, Oct. 2004.

[3] C. H. Wu, C. L. Chiu, and T. G. Ma, "Very compact fully lumped decoupling network for a coupled two-element array," *IEEE Antennas and Wireless Propagation Letters*, vol. 15, pp. 158–161, 2016.

[4] S. C. Chen, Y. S. Wang, and S. J. Chung, "A decoupling technique for increasing the port isolation between two strongly coupled antennas," *IEEE Transactions on Antennas and Propagation*, vol. 56, no. 12, pp. 3650–3658, 2008.

[5] L. Zhao, L. K. Yeung, and K.-L. Wu, "A coupled resonator decoupling network for two-element compact antenna arrays in mobile terminals," *IEEE Transactions on Antennas and Propagation*, vol. 62, no. 5, pp. 2767–2776, 2014.

[6] M. Alibakhshikenari, F. Babaeian, B. S. Virdee et al., "A comprehensive survey on 'various decoupling mechanisms with focus on metamaterial and metasurface principles applicable to SAR and MIMO antenna systems," *IEEE Access*, vol. 8, pp. 192965–193004, 2020.

[7] M. Alibakhshikenari, B. S. Virdee, P. Shukla et al., "Isolation enhancement of densely packed array antennas with periodic MTM-photonic bandgap for SAR and MIMO systems," *IET Microwaves, Antennas & Propagation*, vol. 14, no. 3, pp. 183–188, Feb. 2020.

[8] M. Alibakhshikenari, B. S. Virdee, C. H. See, R. A. Abd-Alhameed, F. Falcone, and E. Limiti, "Surface wave reduction in antenna arrays using metasurface inclusion for MIMO and SAR systems," *Radio Science*, vol. 54, no. 11, pp. 1067–1075, 2019.

[9] M. Alibakhshikenari, B. S. Virdee, C. H. See et al., "Study on isolation improvement between closely-packed patch antenna arrays based on fractal metamaterial electromagnetic bandgap structures," *IET Microwaves, Antennas & Propagation*, vol. 12, no. 14, pp. 2241–2247, 2018.

[10] M. Alibakhshikenari, M. Khalily, B. S. Virdee, C. H. See, R. A. Abd-Alhameed, and E. Limiti, "Mutual coupling suppression between two closely placed microstrip patches using EM-bandgap metamaterial fractal loading," *IEEE Access*, vol. 7, pp. 23606–23614, 2019.

[11] M. Alibakhshikenari, M. Khalily, B. S. Virdee, C. H. See, R. A. Abd-Alhameed, and E. Limiti, "Mutual-coupling isolation using embedded metamaterial EM bandgap decoupling slab for densely packed array antennas," *IEEE Access*, vol. 7, pp. 51827–51840, 2019.

[12] E. Rajo-Iglesias, Ó. Quevedo-Teruel, and L. Inclan-Sanchez, "Mutual coupling reduction in patch antenna arrays by using a planar EBG structure and a multilayer dielectric substrate," *IEEE Transactions on Antennas and Propagation*, vol. 56, no. 6, pp. 1648–1655, 2008.

[13] H. S. Farahani, M. Veysi, M. Kamyab, and A. Tadjalli, "Mutual coupling reduction in patch antenna arrays using a UC-EBG superstrate," *IEEE Antennas and Wireless Propagation Letters*, vol. 9, pp. 57–59, 2010.

[14] X. Yang, Y. Liu, Y. X. Xu, and S. X. Gong, "Isolation enhancement in patch antenna array with fractal UC-EBG structure and cross slot," *IEEE Antennas and Wireless Propagation Letters*, vol. 16, pp. 2175–2178, 2017.

[15] A. Ghalib and M. S. Sharawi, "TCM analysis of defected ground structures for MIMO antenna designs in mobile terminals," *IEEE Access*, vol. 5, pp. 19680–19692, 2017.

[16] C.-M. Luo, J.-S. Hong, and L.-L. Zhong, "Isolation enhancement of a very compact UWB-MIMO slot antenna with two defected ground structures," *IEEE Antennas and Wireless Propagation Letters*, vol. 14, pp. 1766–1769, 2015.

[17] J. OuYang, F. Yang, and Z. M. Wang, "Reducing mutual coupling of closely spaced microstrip MIMO antennas for WLAN application," *IEEE Antennas and Wireless Propagation Letters*, vol. 10, pp. 310–313, 2011.

[18] F.-G. Zhu, J.-D. Xu, and Q. Xu, "Reduction of mutual coupling between closely-packed antenna elements using defected ground structure," *Electronics Letters*, vol. 45, no. 12, p. 601, 2009.

[19] M. M. Bait-Suwailam, O. F. Siddiqui, and O. M. Ramahi, "Mutual coupling reduction between microstrip patch antennas using slotted-complementary split-ring resonators," *IEEE Antennas and Wireless Propagation Letters*, vol. 9, pp. 876–878, 2010.

[20] A. Diallo, C. Luxey, P. Le Thuc, R. Staraj, and G. Kossiavas, "Study and reduction of the mutual coupling between two mobile phone PIFAs operating in the DCS1800 and UMTS bands," *IEEE Transactions on Antennas and Propagation*, vol. 54, no. 11, pp. 3063–3074, 2006.

[21] Y. Wang and Z. Du, "A wideband printed dual-antenna with three neutralization lines for mobile terminals," *IEEE Transactions on Antennas and Propagation*, vol. 62, no. 3, pp. 1495–1500, 2014.

[22] S.-W. Su, C.-T. Lee, and F.-S. Chang, "Printed MIMO-antenna system using neutralization-line technique for wireless USB-dongle applications," *IEEE Transactions on Antennas and Propagation*, vol. 60, no. 2, pp. 456–463, Feb. 2012.

[23] Y. T. Sun, G. S. Cheng, and M. Tian, "Characteristic mode analysis of neutralization line for MIMO antenna design," in *Proceedings of the 2021 International Applied Computational Electromagnetics Society (ACES-China) Symposium*, pp. 1-2, Chengdu, China, July 2021.

[24] R. F. Harrington and J. R. Mautz, "Theory of characteristic modes for conducting bodies," *IEEE Transactions on Antennas and Propagation*, vol. 19, no. 5, pp. 622–628, Sep. 1971.

[25] Q. Wu, W. Su, Z. Li, and D. Su, "Reduction in out-of-band antenna coupling using characteristic mode analysis," *IEEE Transactions on Antennas and Propagation*, vol. 64, no. 7, pp. 2732–2742, 2016.

[26] F. H. Lin and Z. N. Chen, "Low-profile wideband metasurface antennas using characteristic mode analysis," *IEEE Transactions on Antennas and Propagation*, vol. 65, no. 4, pp. 1706–1713, 2017.

[27] Z. Miers and B. K. Lau, "Wideband characteristic mode tracking utilizing far-field patterns," *IEEE Antennas and Wireless Propagation Letters*, vol. 14, pp. 1658–1661, 2015.

[28] Y. Shi, Z. K. Meng, W. Y. Wei, W. Zheng, and L. Li, "Characteristic mode cancellation method and its application for antenna RCS reduction," *IEEE Antennas and Wireless Propagation Letters*, vol. 18, no. 9, pp. 1784–1788, 2019.

[29] J.-F. Lin and L. Zhu, "Bandwidth and gain enhancement of patch antenna based on coupling analysis of characteristic modes," *IEEE Transactions on Antennas and Propagation*, vol. 68, no. 11, pp. 7275–7286, Nov, 2020.

[30] H. Li, Y. Tan, B. K. Lau, Z. Ying, and S. He, "Characteristic mode-based tradeoff analysis of antenna-chassis interactions for multiple antenna terminals," *IEEE Transactions on Antennas and Propagation*, vol. 60, no. 2, pp. 490–502, Feb. 2012.

[31] Y. Chen and C. F. Wang, "Electrically small uav antenna design using characteristic modes," *IEEE Transactions on*

Antennas and Propagation, vol. 62, no. 2, pp. 535–545, Feb. 2014.

[32] S. Wang and H. Arai, "Characteristic modes analysis on neutralizing effect of shorted line for two adjacent PIFA elements," *2014 International Workshop on Antenna Technology (iWAT)*, 2014.

[33] Y. Chen and C.-F. Wang, *Characteristic Modes: Theory and Applications in Antenna Engineering*, Wiley, Hoboken, NJ, USA, 2015.

[34] G. S. Cheng and C.-F. Wang, "A novel periodic characteristic mode analysis method for large-scale finite arrays," *IEEE Transactions on Antennas and Propagation*, vol. 67, no. 12, pp. 7637–7642, 2019.

[35] R. Luomaniemi, P. Ylä-Oijala, A. Lehtovuori, and V. Viikari, "Designing hand-immune handset antennas with adaptive excitation and characteristic modes," *IEEE Transactions on Antennas and Propagation*, vol. 69, no. 7, pp. 3829–3839, 2021.

[36] M. P. Karaboikis, V. C. Papamichael, G. F. Tsachtsiris, C. F. Soras, and V. T. Makios, "Integrating compact printed antennas onto small diversity/MIMO terminals," *IEEE Transactions on Antennas and Propagation*, vol. 56, no. 7, pp. 2067–2078, 2008.

[37] F. A. Dicandia, S. Genovesi, and A. Monorchio, "Analysis of the performance enhancement of MIMO systems employing circular polarization," *IEEE Transactions on Antennas and Propagation*, vol. 65, no. 9, pp. 4824–4835, 2017.

[38] R. Chandel, A. K. Gautam, and K. Rambabu, "Tapered fed compact UWB MIMO-diversity antenna with dual band-notched characteristics," *IEEE Transactions on Antennas and Propagation*, vol. 66, no. 4, pp. 1677–1684, 2018.

[39] S. H. Chae, S.-k. Oh, and S.-O. Park, "Analysis of mutual coupling, correlations, and TARC in WiBro MIMO array antenna," *IEEE Antennas and Wireless Propagation Letters*, vol. 6, pp. 122–125, 2007.